Supplementary Information

Hydrogen bonding of H_2O_2 molecules in crystal structures of alkali metal and tetraethylammonium nitrate peroxosolvates

Alexander G. Medvedev[a], Elena A. Mel'nik[a], Alexey A. Mikhaylov[a], Nikita S. Mayorov[a], Tatiana A. Tripol'skaya[a], Ovadia Lev*[b], Petr V. Prikhodchenko*[a] and Andrei V. Churakov[a]

[a] *N.S. Kurnakov Institute of General and Inorganic Chemistry, Russian Academy of Sciences, Leninskii prosp. 31, 119991 Moscow, Russia*

[b] *Casali Center of Applied Chemistry, Hebrew University of Jerusalem, Jerusalem 9190401, Israel*

Experimental part

Materials

Safety note: Concentrating hydrogen peroxide solutions and working with them requires safety precautions. Handling procedures for concentrated hydrogen peroxide are described in detail (danger of explosion!).[1,2]

Potassium nitrate (99%), rubidium nitrate (99.7%), tetraethylammonium nitrate (98%), hydrogen peroxide (30%) were purchased from Sigma-Aldrich.

Glassware for peroxide rich solutions: All glassware were treated by filling with 1M NaOH for 1 day, then with 1M nitric acid for an additional day, and finally with 10 wt% hydrogen peroxide for a further day. Dichromate or permanganate treatment should be avoided.

Synthesis.

97 wt% hydrogen peroxide was obtained by two step vacuum distillation.[3]

*Potassium nitrate hemiperoxosolvate (**1**)*

0.9 g (8.9 mmol) of potassium nitrate was dissolved in 0.6 mL of 97 wt% hydrogen peroxide. Colorless crystals of **1** were obtained by cooling of prepared solution to -20°C for two days. The crystals were dried on filter paper. Yield 0.253 g (24.1%).

Anal. Calc. for $H_1N_1O_4K_1$ (1): OO (peroxide), 13.54. Found: OO (peroxide), 13.50.

*Rubidium nitrate hemiperoxosolvate (**2**)*

1.6 g (10.8 mmol) of rubidium nitrate was dissolved in 0.5 mL of 97 wt% hydrogen peroxide. Colorless crystals of **2** were obtained by cooling of prepared solution to -20°C overnight. The crystals were dried on filter paper. Yield 0.564 g (31.6%).

Anal. Calc. for $H_1N_1O_4Rb_1$ (1): OO (peroxide), 9.72. Found: OO (peroxide), 9.70.

*Rubidium nitrate hemiperoxosolvate hemihydrate (**3**)*

1.2 g (8.1 mmol) of rubidium nitrate was dissolved in 0.5 mL of 60 wt% hydrogen peroxide. Colorless crystals of **3** were obtained by cooling of prepared solution to 4°C for 2 hrs. The crystals were dried on filter paper. Yield 0.453 g (32.1 %).

Anal. Calc. for $H_2N_1O_{4.5}Rb_1$ (1): OO (peroxide), 9.22. Found: OO (peroxide), 9.12.

Tetraethylammonium nitrate diperoxosolvate (4)

Peroxosolvate **4** were obtained by cooling to -21°C saturated solution (rt) of tetraethylammonium nitrate (1.2 g, 6.2 mmol) in 0.5 mL of 97 wt% hydrogen peroxide. Crystals of **4** are highly unstable and decompose in a few minutes without mother liquor. The latter prevents DSC or FTIR studies.

Characterization

X-ray analysis. Single crystals of **1-4** suitable for X-ray analysis were collected from corresponding mother liquor without additional recrystallization. Experimental intensities were measured on a Bruker SMART APEX II diffractometer (for **1** and **3**) and Bruker D8 Venture machine (for **2** and **4)** using graphite monochromatized MoK_α radiation (λ = 0.71073 Å) in ω-scan mode. Absorption corrections based on measurements of equivalent reflections were applied.[4] The structures were solved by direct methods and refined by full matrix least-squares on F^2 with anisotropic thermal parameters for all non-hydrogen atoms.[5] In all cases, partial substitutional disorder of hydrogen peroxide by water molecules[6–8] was not observed since no residual peaks with an intensity more than 0.25 $e \cdot A^{-3}$ were seen in the hydrogen peroxide molecule regions. In **3**, H_2O_2 molecule was found to be cross-like disordered over two positions with 0.70(9) / 0.30(9) occupancies ratio. All hydrogen atoms were found from difference Fourier synthesis and refined with isotropic thermal parameters. X-ray diffraction studies were performed at the Centre of Shared Equipment of IGIC RAS. Crystal data and details of X-ray analysis are given in Table S1. The crystallographic data have been deposited with the Cambridge Crystallographic Data Centre as supplementary publications under the CCDC numbers 2361132 (**1**), 2361133 (**2**), 2364418 (**3**) and 2361134 (**4**).

Elemental analysis. Peroxide content was determined by permanganometric titration.[2]

X-ray powder diffraction measurements were performed on a D8 Advance diffractometer (Bruker AXS, Karlsruhe, Germany) with a goniometer radius of 280 mm. The powder samples were filled into low background quartz sample holders without grinding to prevent sample decomposition. XRD patterns in the range 10˚ to 50˚ 2θ were recorded at room temperature using CuKα radiation (λ=1.5418 Å) under the following measurement conditions: tube voltage of 40 kV, tube current of 40 mA, step size 0.02˚ 2θ, counting time 1 s/step. XRD patterns were processed by DiffracPlus software.

FTIR spectra were recorded on a JASCO FT/IR-4600 spectrometer.

Differential thermal analysis (DTA) and **thermogravimetry analysis** (TGA) were performed on simultaneous thermal analyzer, DTG-60 (Shimadzu). All experiments were carried out under argon flow at a heating rate of 10 °C/min.

Solid-state DFT calculations.

The space groups and unit cell parameters of **1**, **2**, **4** obtained in the single-crystal X-ray studies are fixed and structural relaxations are limited to the positional parameters of atoms. The atomic positions from scXRD experiment, CCDC GAVSEF,[9] GAVRUU,[9] WUTKUT04,[10] and BOHLOC[11] refcodes are used as the starting point in the solid-state DFT computations. Density functional theory computations with periodic boundary conditions (solid-state DFT) were performed in the Crystal23 software package[12] using B3LYP, PBE and PBE0 functionals and the localized basis set 6-31G** and pob-TZVP basis set.[13,14] The London dispersion interactions were taken into account by the D3 correction with Becke-Jones damping. The mixing coefficient of Hartree-Fock/Kohn-Sham matrices is set to 25%. Tolerance on energy controlling the self-consistent field convergence for geometry optimizations and frequencies computations is set to 10^{-}

^{10} and 10^{-11} Hartree, respectively. The shrinking factor of the reciprocal space net is set to 3. The optimized structures are found to correspond to the minimum point on the potential energy surface.

The Bader analysis of the periodic electron density was performed using Topond21.[15]

The energy of intermolecular H-bonds E_{HB} is evaluated according to ref. [16] as:

$$E_{HB} = 1126 \cdot G_b \quad (1)$$

where G_b is the positively-defined local electronic kinetic energy density at the H···O bond critical point.[17] The Espinosa approach gives reasonable results for energies of intermolecular H-bonds and other non-covalent interactions in organic crystals varying from 2.0 to 50 kJ mol^{-1}.[18]

The enthalpy of H-bond ΔH_{HB} was estimated using the Rozenberg approach[19]:

$$-\Delta H_{HB}\ [\text{kJ/mol}] = 0.134 \cdot R(\text{H}\cdots\text{O})^{-3.05}, \quad (2)$$

where the R(H···O) is the H···O distance (nm). Herein, the R(H…O) distances are obtained as a result of geometry optimization of crystal structures data obtained from SCXRD. The empirical correlation (2) for molecular crystals describes the $-\Delta H_{HB}$ values of intermolecular H-bonds of different strengths and types, including ionic or charged fragments, in the range from 10 to 80 kJ mol^{-1} with the accuracy of several kJ mol^{-1}.[19]

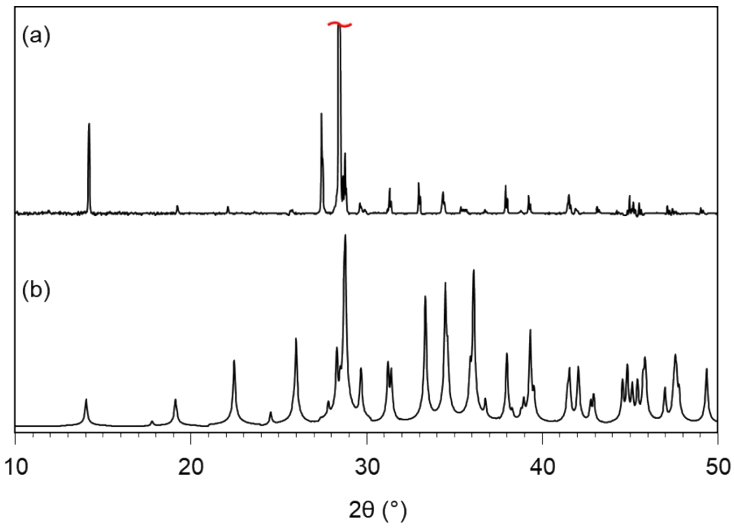

Figure S1. Experimental (a) and calculated (b) powder diffractograms of peroxosolvate **1**.

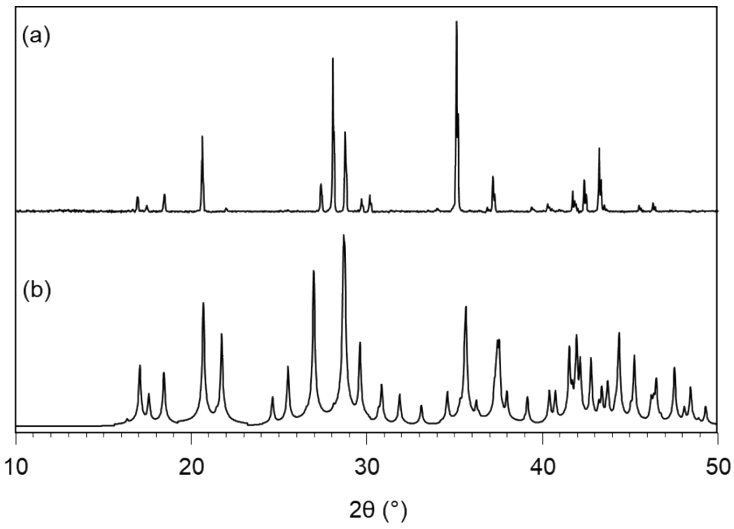

Figure S2. Experimental (a) and calculated (b) powder diffractograms of peroxosolvate **2**.

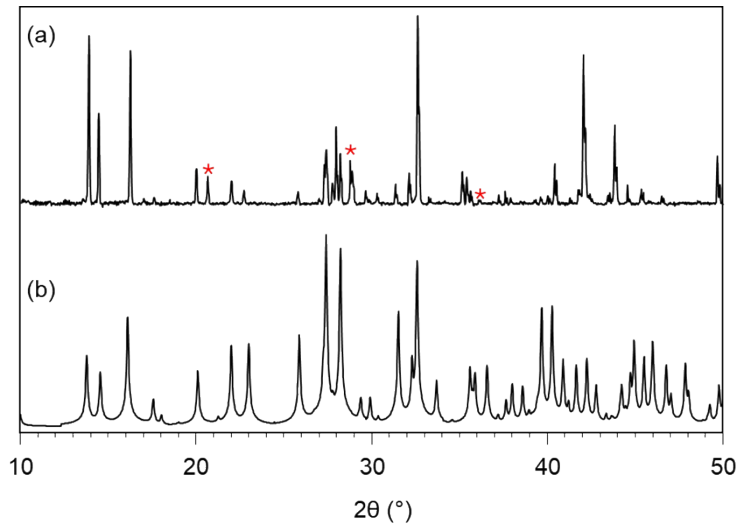

Figure S3. Experimental (a) and calculated (b) powder diffractograms of peroxosolvate **3**. * - $RbNO_3$ admixture.

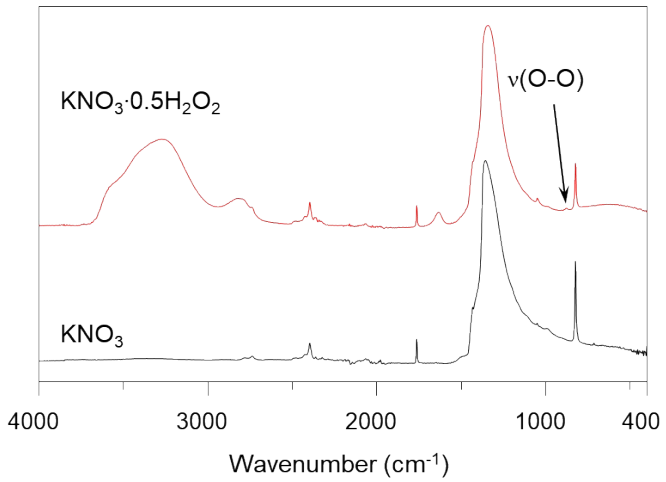

Figure S4. FTIR spectra of potassium nitrate and peroxosolvate **1**.

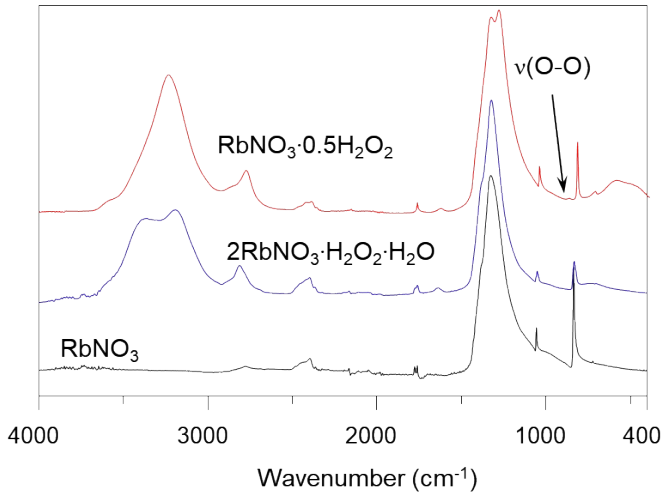

Figure S5. FTIR spectra of rubidium nitrate and peroxosolvates **2** and **3**.

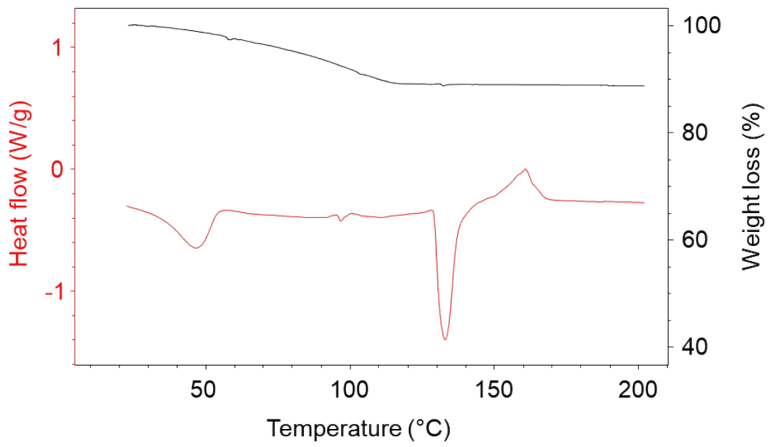

Figure S6. TG and DSC curves of compound **1**.

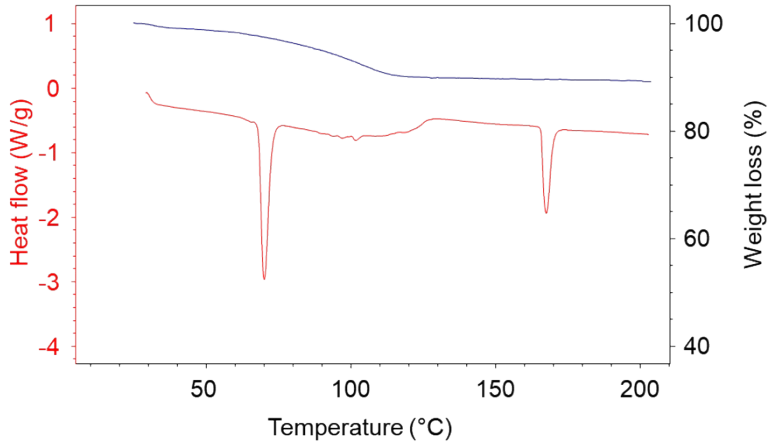

Figure S7. TG and DSC curves of compound **2**.

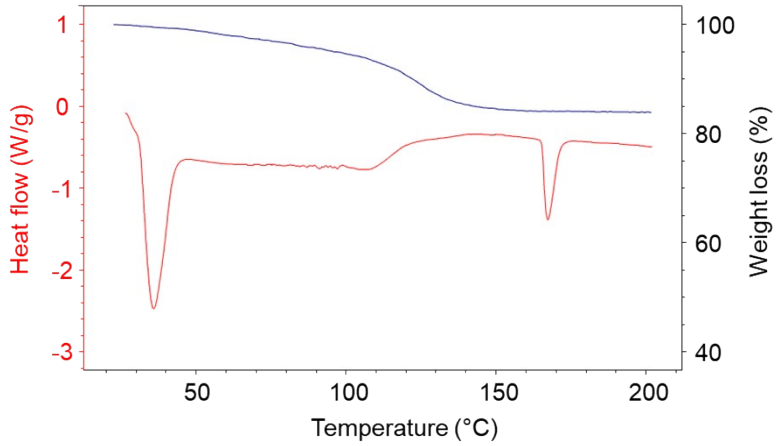

Figure S8. TG and DSC curves of compound **3**.

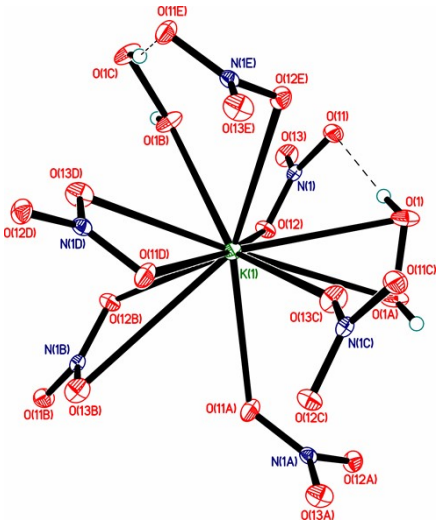

Figure S9. Environment of potassium cation in the crystal structure of **1**. Displacement ellipsoids are shown at 50% probability level. Hydrogen bonds are drawn by dashed lines.

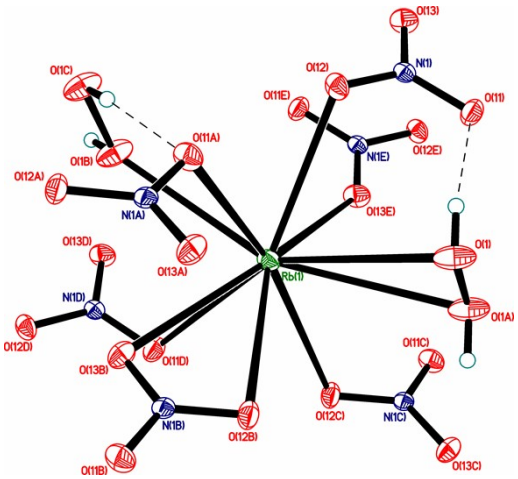

Figure S10. Environment of rubidium cation in the crystal structure of **2**. Displacement ellipsoids are shown at 50% probability level. Hydrogen bonds are drawn by dashed lines.

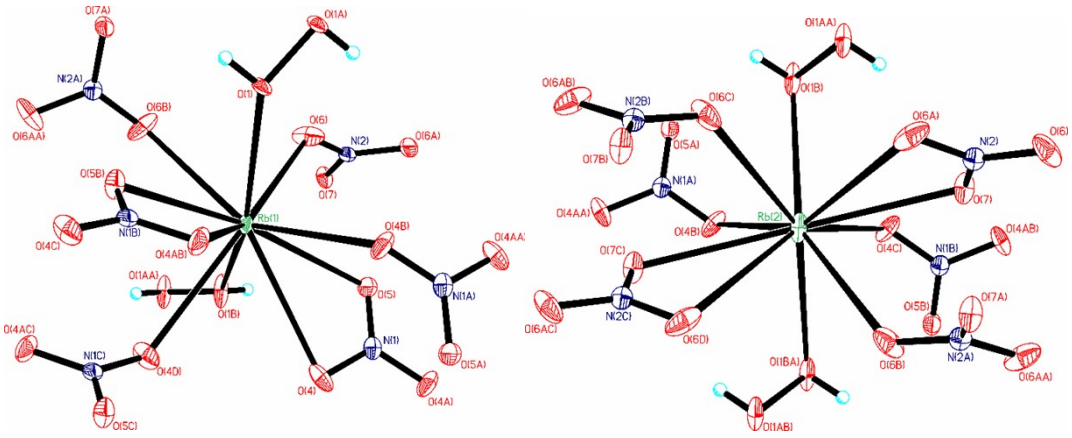

Figure S11. Environment of rubidium cations in the crystal structure of **3**. Displacement ellipsoids are shown at 50% probability level. Only major components of H_2O_2 disorder are shown.

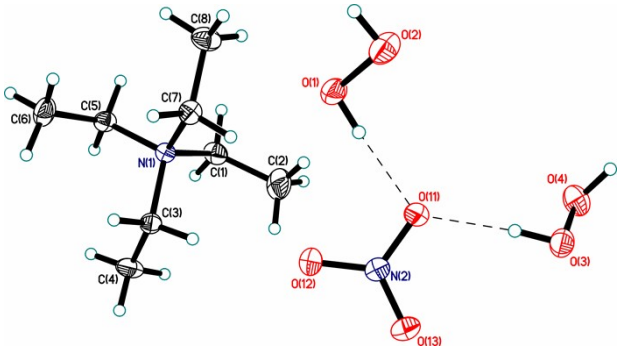

Figure S12. Asymmetric unit in the crystal structure of **4**. Displacement ellipsoids are shown at 50% probability level. Hydrogen bonds are drawn by dashed lines.

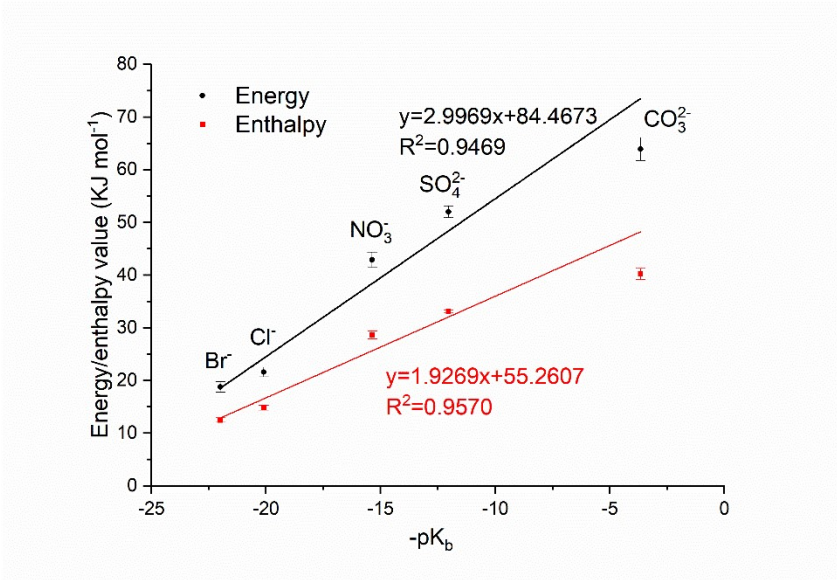

Figure S13. Correlation of the energy/enthalpy values of hydrogen bonds of H_2O_2 versus the $-pK_b$ levels of the conjugated acid of the acceptor anions obtained at B3LYP-D3/pob-TZVP level of theory.

Table S1. Crystal data and details of X-ray analysis.

	1	**2**	**3**	**4**
Formula	$H_1K_1N_1O_4$	$H_1N_1O_4Rb_1$	$H_4N_2O_9Rb_2$	$C_8H_{24}N_2O_7$
*F*w	118.12	164.49	346.99	260.29
colour, habit	colourless, prism	colourless, prism	colourless, prism	colourless, prism
cryst size (mm)	0.40×0.30×0.20	0.08×0.06×0.04	0.25×0.15×0.08	0.25×0.20×0.20
temperature (K)	100	150	120	100
crystal system	monoclinic	monoclinic	orthorhombic	orthorhombic
space group	$P2_1/c$	$P2_1/n$	*I*bam	*P*bca
a (Å)	6.9591(9)	6.7050(3)	12.1429(11)	12.3185(4)
b (Å)	6.8466(8)	8.1533(3)	12.8212(11)	14.6896(5)
c (Å)	8.0046(10)	7.2160(2)	10.9801(9)	15.1162(5)
β (deg)	115.264(4)	92.7189(13)	90	90
V (Å^3)	344.91(7)	394.04(3)	1709.5(3)	2735.33(16)
Z	4	4	8	8
D_c (g·cm^{-3})	2.275	2.773	2.697	1.264
μ (mm^{-1})	1.392	12.436	11.482	0.109
F(000)	236	308	1312	1136
θ range (deg)	3.24 to 30.00	3.77 to 30.00	2.31 to 28.99	2.54 to 27.00
refl collcd	4042	6218	9574	33352
indep reflns / R_{int}	991 / 0.016	1150 / 0.025	1199 / 0.070	2988 / 0.037
reflns $I>2\sigma(I)$	964	1068	817	2599
No of param	60	60	88	250
GooF on F^2	1.133	1.085	1.079	1.039
R_1 ($I>2\sigma(I)$)	0.0149	0.0145	0.0360	0.0346
wR_2(all data)	0.0369	0.0309	0.0735	0.0896
largest diff peak / hole (e·Å^{-3})	0.25 / -0.26	0.43 / -0.34	0.68 / -0.77	0.24 / -0.26
CCDC number	2361132	2361133	2364418	2361134

Table S2 Experimental and optimized parameters of the O-H…O hydrogen bonds of H_2O_2 molecules in **1**, **2** and **4** with pob-TZVP basis set.

Fragment[a)]	d(O…O), Å		d(H…O), Å		∠(O-H…O), °	
	Exp	Calcd[b)]	Exp	Calcd[b)]	Exp	Calcd[b)]
1						
O(1)-H(1)…O(11)	2.759(1)	2.678/ 2.648/ 2.670	1.91(1)	1.687/ 1.639/ 1.680	167(1)	170/ 170/ 170
2						
O(1)-H(1)…O(11)	2.762(2)	2.684/ 2.662/ 2.675	1.96(2)	1.699/ 1.656/ 1.691	162(2)	170/ 168/ 167
4						
O(1)-H(1)…O(11)	2.757(1)	2.742/ 2.739/ 2.738	1.88(2)	1.750/ 1.733/ 1.748	174(2)	177/ 177/ 176
O(3)-H(3)…O(11)	2.750(1)	2.720/ 2.705/ 2.722	1.85(2)	1.722/ 1.690/ 1.726	174(2)	176/ 175/ 176
O(2)-H(2)…O(3)	2.807(1)	2.736/ 2.712/ 2.731	1.95(2)	1.741/ 1.699/ 1.738	166(2)	176/ 176/ 176
O(4)-H(4)…O(12)	2.794(1)	2.747/ 2.732/ 2.744	1.87(2)	1.767/ 1.738/ 1.772	168(2)	168/ 167/ 167

[a)] See Figs. 1, 2 and 4 for atom labeling in **1**, **2** and **4**, respectively; [b)] Values obtained with B3LYP-D3/PBE-D3/PBE0-D3 functionals and pob-TZVP basis set.

Table S3 Computed values of the electron density, ρ_b, the local electronic kinetic energy density, G_b at the O-H…O hydrogen bonds of H_2O_2 molecules critical point and the energy/enthalpy values E_{HB} /-H_{HB} evaluated using Eqs. S1, S2 in **1**, **2** and **4**.

Fragment [a]	E_{HB}[b] (kJ mol^{-1}) [d]	-H_{HB}[c] (kJ mol^{-1}) [d]
1		
O(1)-H(1)…O(11)	46.7/ 50.6/ 47.9	30.5/ 33.3/ 30.9
2		
O(1)-H(1)…O(11)	45.6/ 48.8/ 46.9	29.9/ 32.3/ 30.3
4		
O(1)-H(1)…O(11)	40.6/ 41.0/ 41.1	27.3/ 28.1/ 27.4
O(3)-H(3)…O(11)	42.7/ 44.5/ 42.6	28.7/ 30.3/ 28.5
O(2)-H(2)…O(3)	41.2/ 44.0/ 41.8	27.7/ 29.9/ 27.9
O(4)-H(4)…O(12)	38.9/ 40.3/ 38.8	26.5/ 27.9/ 26.3

[a] See Figs. 1, 2 and 4 for atom labeling in **1**, **2** and **4**, respectively; [b] see Eq. S1; [c] see Eq. S2; [d] Values obtained with B3LYP-D3/PBE-D3/PBE0-D3 functionals and pob-TZVP basis set.

Table S4. Computed values of the electron density, ρ_b, the Laplacian of the electron density, $\nabla^2\rho_b$, the local electronic kinetic energy density, G_b at the K…O critical point and energy, E_{KO}, evaluated using Eq. (1) in **1** (B3LYP-D3/6-31G** level of theory).

R(K…O), Å	ρ_b (a.u.)	$\nabla^2\rho_b$ (a.u.)	G_b (a.u.)	E_{KO}, kJ mol^{-1}
K…O(H)-O(H)				
3.017	0.0086	0..0403	0.0083	9.3
3.031	0.0083	0.0402	0.0082	9.3
2.803	0.0128	0.0609	0.0128	14.4
K…ONO$_2$				
2.749	0.0131	0.0664	0.0137	15.4
2.852	0.0123	0.0548	0.0116	13.1
2.834	0.0119	0.0549	0.0116	13.0
2.857	0.0123	0.0544	0.0116	13.0
2.929	0.0109	0.0474	0.0100	11.3
2.933	0.0100	0.0442	0.0092	10.4
2.975	0.0099	0.0431	0.0090	10.2

Table S5. Computed values of the electron density, ρ_b, the Laplacian of the electron density, $\nabla^2\rho_b$, the local electronic kinetic energy density, G_b at the Rb…O critical point and energy, E_{RbO}, evaluated using Eq. (1) in **2** (B3LYP-D3/6-31G** level of theory).

R(Rb…O), Å	ρ_b (a.u.)	$\nabla^2\rho_b$ (a.u.)	G_b (a.u.)	E_{RbO}, kJ mol^{-1}
Rb…O(H)-O(H)				
3.070	0.0099	0.0420	0.0091	10.3
3.213	0.0078	0.0337	0.0072	8.1
Rb…ONO$_2$				
2.845	0.0156	0.0667	0.0148	16.7
2.956	0.0128	0.0526	0.0117	13.2
2.988	0.0122	0.0502	0.0112	12.6
2.994	0.0121	0.0493	0.0101	12.4
3.013	0.0115	0.0472	0.0105	11.8
3.013	0.0126	0.0499	0.0113	12.7
3.044	0.0117	0.0472	0.0106	11.9

Table S6. Experimental and optimized parameters of the O-H…A (A=O, Br) H-bonds in Et_4N^+ Br^- $2H_2O_2$

Fragment[a)]	d(O…A), Å		d(H…A), Å		∠(O-H…A), °	
	Exp	Calcd[b)]	Exp	Calcd[b)]	Exp	Calcd[b)]
O(1)-H(1)…O(4)	2.818(3)	2.766/2.757	2.07(4)	1.791/1.769	168(5)	170/169
O(2)-H(2)…Br(1)	3.288(2)	3.317/3.312	2.48(4)	2.333/2.318	161(6)	176/175
O(3)-H(3)…Br(1)	3.238(2)	3.229/3.212	2.40(4)	2.251/2.224	166(3)	170/168
O(4)-H(4)…Br(1)	3.235(2)	3.239/3.226	2.43(3)	2.250/2.225	175(3)	176/174

[a)] See Fig. 1, Table 1 doi: 10.1039/d1ce01476e for atom labeling; [b)] Values obtained with B3LYP-D3/PBE-D3 functionals and 6-31G** basis set.

Table S7. Computed values of the electron density, ρ_b, the local electronic kinetic energy density, G_b at the O-H…A (A=O, Br) hydrogen bonds critical point and the energy/enthalpy values E_{HB} /H_{HB} evaluated using Eqs. S1, S2 in Et_4N^+ Br^- $2H_2O_2$.

Fragment[a)]	ρ_b (a.u.)	G_b (a.u.)	E_{HB}[b)]	H_{HB}[c)]
			(kJ mol^{-1})	
O(1)-H(1)…O(4)	0.0364/0.0396[d)]	0.0270/0.0278	**30.4/31.3**	**25.4/26.4**
O(2)-H(2)…Br(1)	0.0231/0.0245	0.0124/0.0126	**14.0/14.2**	**11.3/11.6**
O(3)-H(3)…Br(1)	0.0276/0.0299	0.0148/0.0153	**16.6/17.2**	**12.7/13.1**
O(4)-H(4)…Br(1)	0.0274/0.0296	0.0145/0.0149	**16.3/16.8**	**12.7/13.1**

[a)] See Fig. 1, Table 1 doi: 10.1039/d1ce01476e for atom labeling; [b)] see Eq. S1; [c)] see Eq. S2; [d)] Values obtained with B3LYP-D3/PBE-D3 functionals and 6-31G** basis set.

Table S8. Experimental and optimized parameters of the O-H…A (A=O, Cl) H-bonds in Et_4N^+ Cl^- $2H_2O_2$

Fragment[a)]	d(O…A), Å		d(H…A), Å		∠(O-H…A), °	
	Exp	Calcd[b)]	Exp	Calcd[b)]	Exp	Calcd[b)]
O(1)-H(1)…O(4)	2.833(2)	2.775/2.763	1.97(3)	1.800/1.775	173(3)	170/169
O(2)-H(2)…Cl(1)	3.152(2)	3.209/3.209	2.26(3)	2.226/2.216	172(3)	175/173
O(3)-H(3)…Cl(1)	3.118(1)	3.127/3.110	2.30(3)	2.161/2.136	170(3)	165/164
O(4)-H(4)…Cl(1)	3.095(1)	3.117/3.107	2.21(2)	2.123/2.107	173(3)	174/173

[a)] See Fig. 1, Table 1 doi: 10.1039/d1ce01476e for atom labeling; [b)] Values obtained with B3LYP-D3/PBE-D3 functionals and 6-31G** basis set.

Table S9. Computed values of the electron density, ρ_b, the local electronic kinetic energy density, G_b at the O-H…A (A=O, Cl) hydrogen bonds critical point and the energy/enthalpy values E_{HB} /H_{HB} evaluated using Eqs. S1, S2 in Et_4N^+ Cl^- $2H_2O_2$.

Fragment[a)]	ρ_b (a.u.)	G_b (a.u.)	E_{HB}[b)]	H_{HB}[c)]
			(kJ mol^{-1})	
O(1)-H(1)…O(4)	0.0357/0.0392[d)]	0.0263/0.0273	**29.7/30.7**	**25.0/26.1**
O(2)-H(2)…Cl(1)	0.0234/0.0244	0.0144/0.0145	**16.2/16.3**	**13.1/13.3**
O(3)-H(3)…Cl(1)	0.0288/0.0310	0.0174/0.0179	**19.6/20.2**	**14.3/14.9**
O(4)-H(4)…Cl(1)	0.0271/0.0293	0.0167/0.0174	**18.8/19.6**	**15.1/15.5**

[a)] See Fig. 1, Table 1 doi: 10.1039/d1ce01476e for atom labeling; [b)] see Eq. S1; [c)] see Eq. S2; [d)] Values obtained with B3LYP-D3/PBE-D3 functionals and 6-31G** basis set.

Table S10. Experimental and optimized parameters of the O-H…O hydrogen bonds in $Na_2CO_3{\cdot}1.5H_2O_2$.

Fragment[a)]	d(O…A), Å		d(H…A), Å		∠(O-H…A), °	
	Exp	Calcd[b)]	Exp	Calcd[b)]	Exp	Calcd[b)]
O(11)-H(11)…O(1)	2.602(1)	2.587/2.568	1.58(1)	1.574/1.534	170(1)	171/172
O(12)-H(12)…O(2)	2.595(1)	2.584/2.564	1.64(1)	1.567/1.526	169(1)	174/174
O(31)-H(31)…O(3)[c)]	2.557(1)	2.548/2.537	1.62(1)	1.529/1.499	157(1)	176/176

[a)] See Fig. 8, Table 3 doi: 10.1107/S0108768103012291 for atom labeling; [b)] Values obtained with B3LYP-D3/PBE-D3 functionals and 6-31G** basis set; [c)] Only the major component of disorder was considered for periodic calculations.

Table S11. Computed values of the electron density, ρ_b, the local electronic kinetic energy density, G_b at the O-H…O hydrogen bonds critical point and the energy/enthalpy values E_{HB} /H_{HB} evaluated using Eqs. S1, S2 in $Na_2CO_3{\cdot}1.5H_2O_2$.

Fragment[a)]	ρ_b (a.u.)	G_b (a.u.)	E_{HB}[b)]	H_{HB}[c)]
			(kJ mol^{-1})	
O(11)-H(11)…O(1)	0.0636/0.0722[d)]	0.0462/0.0503	**52.0/56.6**	**37.7/40.8**
O(12)-H(12)…O(2)	0.0646/0.0736	0.0471/0.0515	**53.0/58.0**	**38.2/41.4**
O(31)-H(31)…O(3)[c)]	0.0708/0.0784	0.0631/0.0564	**59.8/63.5**	**41.1/43.7**

[a)] See Fig. 8, Table 3 doi: 10.1107/S0108768103012291 for atom labeling; [b)] see Eq. S1; [c)] see Eq. S2; [d)] Values obtained with B3LYP-D3/PBE-D3 functionals and 6-31G** basis set; [e)] Only the major component of disorder was considered for periodic calculations.

Table S12. Experimental and optimized parameters of the D-H…O (D=O, N) hydrogen bonds of H_2O_2 molecules in $(CH_6N_3)_2^+ SO_4^{2-} \cdot H_2O_2$.

Fragment[a)]	d(O…A), Å		d(H…A), Å		∠(O-H…A), °	
	Exp	Calcd[b)]	Exp	Calcd[b)]	Exp	Calcd[b)]
O(1)-H(1)…O(12)	2.681(2)	2.669/2.671	1.81(3)	1.686/1.676	167(2)	169/169
O(2)-H(2)…O(11)	2.668(2)	2.644/2.643	1.83(3)	1.673/1.660	167(2)	165/165
N(32)-H(322)…O(2)	3.082(2)	3.006/2.966	2.28(3)	2.048/1.990	154(2)	156/157
N(31)-H(31)…O(1)	2.896(2)	2.849/2.836	2.00(3)	1.837/1.815	178(3)	170/169

[a)] See Fig. 2 doi: 10.1002/prep.201800177 for atom labeling; [b)] Values obtained with B3LYP-D3/PBE-D3 functionals and 6-31G** basis set.

Table S13. Computed values of the electron density, ρ_b, the local electronic kinetic energy density, G_b at the D-H…O (D=O, N) hydrogen bonds of H_2O_2 molecules critical point and the energy/enthalpy values E_{HB} /H_{HB} evaluated using Eqs. S1, S2 in $(CH_6N_3)_2^+ SO_4^{2-} \cdot H_2O_2$.

Fragment[a)]	ρ_b (a.u.)	G_b (a.u.)	E_{HB}[b)]	H_{HB}[c)]
			(kJ mol^{-1})	
O(1)-H(1)…O(12)	0.0453/0.0478[d)]	0.0347/0.0350	**39.1/39.4**	**30.6/31.1**
O(2)-H(2)…O(11)	0.0481/0.0509	0.0372/0.0377	**41.9/42.5**	**31.3/32.0**
N(32)-H(322)…O(2)	0.0227/0.0263	0.0160/0.0175	**18.0/19.8**	**16.9/18.4**
N(31)-H(31)…O(1)	0.0343/0.0371	0.0255/00263	**28.7/29.6**	**23.5/24.4**

[a)] See Fig. 2 doi: 10.1002/prep.201800177 for atom labeling; [b)] see Eq. S1; [c)] see Eq. S2; [d)] Values obtained with B3LYP-D3/PBE-D3 functionals and 6-31G** basis set.

Table S14. Experimental and optimized parameters, energy and enthalpy values of hydrogen peroxide O-H…A (A=O, Br, Cl) H-bonds in Et_4N^+ Br^- $2H_2O_2$, Et_4N^+ Cl^- $2H_2O_2$, $Na_2CO_3{\cdot}1.5H_2O_2$ and $(CH_6N_3)_2^+$ SO_4^{2-} · H_2O_2 peroxosolvates at the B3LYP-D3/pob-TZVP level of theory.

Fragment	d(O…A), Å		d(H…A), Å		E_{HB}[b]	H_{HB}[c]
	Exp	Calcd[a]	Exp	Calcd[a]		
Et_4N^+ Br^- $2H_2O_2$						
O(2)-H(2)…Br(1)	3.288(2)	3.299	2.48(4)	2.310	16.8	11.7
O(3)-H(3)…Br(1)	3.238(2)	3.227	2.40(4)	2.246	19.5	12.7
O(4)-H(4)…Br(1)	3.235(2)	3.225	2.43(3)	2.226	20.0	13.1
Et_4N^+ Cl^- $2H_2O_2$						
O(2)-H(2)…Cl(1)	3.152(2)	3.174	2.26(3)	2.185	20.0	13.9
O(3)-H(3)…Cl(1)	3.118(1)	3.121	2.30(3)	2.115	21.7	15.3
O(4)-H(4)…Cl(1)	3.095(1)	3.108	2.21(2)	2.111	23.1	15.4
$Na_2CO_3{\cdot}1.5H_2O_2$						
O(11)-H(11)…O(1)	2.602(1)	2.581	1.58(1)	1.557	61.3	39.0
O(12)-H(12)…O(2)	2.595(1)	2.578	1.64(1)	1.551	62.2	39.4
O(31)-H(31)…O(3)[c]	2.557(1)	2.543	1.62(1)	1.516	68.2	42.3
$(CH_6N_3)_2^+$ SO_4^{2-} · H_2O_2						
O(1)-H(1)…O(12)	2.681(2)	2.640	1.81(3)	1.647	50.9	32.8
O(2)-H(2)…O(11)	2.668(2)	2.622	1.83(3)	1.638	53.1	33.4

[a] Values obtained with B3LYP-D3/pob-TZVP level of theory; [b] see Eq. S1; [c] see Eq. S2.

References

(1) Maass, O.; Hatcher, W. H. The PROPERTIES OF PURE HYDROGEN PEROXIDE. I. *J. Am. Chem. Soc.* **1920**, *42* (12), 2548–2569. https://doi.org/10.1021/ja01457a013.

(2) Schumb, W. C.; Satterfield, C. N.; Wentworth, R. L. *Hydrogen Peroxide*; Reinhold Publishing Corporation: New York, 1955. https://doi.org/10.1002/jps.3030450224.

(3) Medvedev, A. G.; Egorov, P. A.; Mikhaylov, A. A.; Belyaev, E. S.; Kirakosyan, G. A.; Gorbunova, Y. G.; Filippov, O. A.; Belkova, N. V.; Shubina, E. S.; Brekhovskikh, M. N.; Kirsanova, A. A.; Babak, M. V.; Lev, O.; Prikhodchenko, P. V. Synergism of Primary and Secondary Interactions in a Crystalline Hydrogen Peroxide Complex with Tin. *Nat. Commun.* **2024**, *15* (1), 5758. https://doi.org/10.1038/s41467-024-50164-9.

(4) Krause, L.; Herbst-Irmer, R.; Sheldrick, G. M.; Stalke, D. Comparison of Silver and Molybdenum Microfocus X-Ray Sources for Single-Crystal Structure Determination. *J. Appl. Crystallogr.* **2015**, *48* (1), 3–10. https://doi.org/10.1107/S1600576714022985.

(5) Sheldrick, G. M. Crystal Structure Refinement with SHELXL. *Acta Crystallogr. Sect. C Struct. Chem.* **2015**, *71*, 3–8. https://doi.org/10.1107/S2053229614024218.

(6) Pedersen, B. F. The Observed Shortening of the Oxygen–Oxygen Bond in the Hydrogen Peroxide Molecule in Solids. *Acta Crystallogr. Sect. B Struct. Crystallogr. Cryst. Chem.* **1972**, *28* (4), 1014–1016. https://doi.org/10.1107/S0567740872003620.

(7) Laus, G.; Kahlenberg, V.; Wurst, K.; Lörting, T.; Schottenberger, H. Hydrogen Bonding in the Perhydrate and Hydrates of 1,4-Diazabicyclo[2.2.2]Octane (DABCO). *CrystEngComm* **2008**, *10* (11), 1638. https://doi.org/10.1039/b807303a.

(8) Churakov, A. V.; Prikhodchenko, P. V.; Howard, J. A. K. The Preparation and Crystal Structures of Novel Perhydrates Ph4X+Hal–·nH2O2: Anionic Hydrogen-Bonded Chains Containing Hydrogen Peroxide. *CrystEngComm* **2005**, *7* (110), 664. https://doi.org/10.1039/b511834d.

(9) Navasardyan, M. A.; Bezzubov, S. I.; Medvedev, A. G.; Prikhodchenko, P. V.; Churakov, A. V. Novel Peroxosolvates of Tetraalkylammonium Halides: The First Case of Layers Containing Hydrogen-Bonded Peroxide Molecules. *CrystEngComm* **2022**, *24* (1), 38–42. https://doi.org/10.1039/D1CE01476E.

(10) Pritchard, R. G.; Islam, E. Sodium Percarbonate between 293 and 100 K. *Acta Crystallogr. Sect. B Struct. Sci.* **2003**, *59* (5), 596–605. https://doi.org/10.1107/S0108768103012291.

(11) Churakov, A. V.; Medvedev, A. G.; Navasardyan, M. A.; Grishanov, D. A.; Prikhodchenko, P. V. The Crystal Structure of Guanidinium Sulphate Hemiperoxosolvate. *Propellants, Explos. Pyrotech.* **2018**, *43* (9), 859–861. https://doi.org/10.1002/prep.201800177.

(12) Erba, A.; Desmarais, J. K.; Casassa, S.; Civalleri, B.; Donà, L.; Bush, I. J.; Searle, B.; Maschio, L.; Edith-Daga, L.; Cossard, A.; Ribaldone, C.; Ascrizzi, E.; Marana, N. L.; Flament, J.-P.; Kirtman, B. CRYSTAL23: A Program for Computational Solid State Physics and Chemistry. *J. Chem. Theory Comput.* **2023**, *19* (20), 6891–6932. https://doi.org/10.1021/acs.jctc.2c00958.

(13) Vilela Oliveira, D.; Laun, J.; Peintinger, M. F.; Bredow, T. BSSE-correction Scheme for Consistent Gaussian Basis Sets of Double- and Triple-zeta Valence with Polarization Quality for Solid-state Calculations. *J. Comput. Chem.* **2019**, *40* (27), 2364–2376.

https://doi.org/10.1002/jcc.26013.

(14) Laun, J.; Bredow, T. <scp>BSSE-corrected</Scp> Consistent Gaussian Basis Sets of <scp>triple-zeta</Scp> Valence with Polarization Quality of the Fifth Period for <scp>solid-state</Scp> Calculations. *J. Comput. Chem.* **2022**, *43* (12), 839–846. https://doi.org/10.1002/jcc.26839.

(15) Cossard, A.; Desmarais, J. K.; Casassa, S.; Gatti, C.; Erba, A. Charge Density Analysis of Actinide Compounds from the Quantum Theory of Atoms in Molecules and Crystals. *J. Phys. Chem. Lett.* **2021**, *12* (7), 1862–1868. https://doi.org/10.1021/acs.jpclett.1c00100.

(16) Mata, I.; Alkorta, I.; Espinosa, E.; Molins, E. Relationships between Interaction Energy, Intermolecular Distance and Electron Density Properties in Hydrogen Bonded Complexes under External Electric Fields. *Chem. Phys. Lett.* **2011**, *507* (1–3), 185–189. https://doi.org/10.1016/j.cplett.2011.03.055.

(17) Bader, R. F. W. A Quantum Theory of Molecular Structure and Its Applications. *Chem. Rev.* **1991**, *91* (5), 893–928. https://doi.org/10.1021/cr00005a013.

(18) Medvedev, A. G.; Churakov, A. V.; Prikhodchenko, P. V.; Lev, O.; Vener, M. V. Crystalline Peroxosolvates: Nature of the Coformer, Hydrogen-Bonded Networks and Clusters, Intermolecular Interactions. *Molecules* **2021**, *26* (1), 26. https://doi.org/10.3390/molecules26010026.

(19) Rozenberg, M.; Loewenschuss, A.; Marcus, Y. An Empirical Correlation between Stretching Vibration Redshift and Hydrogen Bond Length. *Phys. Chem. Chem. Phys.* **2000**, *2* (12), 2699–2702. https://doi.org/10.1039/b002216k.